Snap-through and local buckling interaction in a timber dome: Bracing system vs. connection stiffness

September 25th - 28th, 2017
INTERFACES
architecture . engineering . science IASS 2017 hamburg

Proceedings of the IASS Annual Symposium 2017
"Interfaces: architecture . engineering . science"
September 25 - 28th, 2017, Hamburg, Germany
Annette Bögle, Manfred Grohmann (eds.)

Snap-through and local buckling interaction in a timber dome: Bracing system vs. connection stiffness

Amedeo MANUELLO*, Fabio BAZZUCCHI.[a], Alberto CARPINTERI[a]

* Department of Structural, Geotechnical and Building Engineering-
Politecnico di Torino
Corso Duca degli Abruzzi 24, 10129 Torino
amedeo.manuellobertetto@polito.it

[a] Department of Structural, Geotechnical and Building Engineering-
Politecnico di Torino

Abstract

In the present paper, the stability of an existent single layer timber dome has been studied considering different loading configurations and increasing the yieldingness of the connecting nodes. In addition, the amplitude and the shape of geometrical imperfections have been applied as referred to the buckling modes of each constituting module, a Von-Mises arch. Numerical analyses have been conducted with local displacement controls, with a co-rotational formulation to take into account the geometric nonlinearity. Results evidenced that the dome is sensitive to the interaction between different instability phenomena for particular configurations and connection stiffness reduction (yieldingness). The effect of the existent bracing system has been evaluated, evidencing that its presence is also unfavorable for determined configurations.

Keywords: local buckling, snap-through, timber dome, geometric nonlinearity, imperfection pattern, bracing system, connection stiffness.

1. Introduction

Concerning the stability of reticulated domes, interaction between buckling and snap-through establishes a localized critic condition that could lead the structures towards catastrophic progressive collapses [1-3]. Because of the geometric nonlinearity and the unknown imperfection patterns, the evaluation of the ultimate load became a research challenge in Structural Mechanics. In particular, the stability condition of large span roof is one of the most important check to be evaluated [4-7]. An other fundamental task is represented by the stiffness loss (yielding) localized in the nodes connecting the beams [3-5]. This problem characterizing the in-service lifetime of steel and reinforced concrete spatial structures, appeared to be even more evident and serious in the case of reticulated timber roof [4-7]. In the present paper, the geometrically non-linear behaviour of an existing timber geodesic dome was analyzed considering the evolution (depletion) of the stiffness in the nodes of the structure. At the same time the amplitude and the shape of imperfections have been applied as referred to the buckling modes of each constituting module (Von-Mises arch) [1,2]. The considered architecture was represented by the *Maria Piantanida* sport palace, near Milan, in the north-western of Italy (Fig. 1a). The structure has been built in 1997, and is able to host up to 5000 spectators. The roof structure is realized by a geodesic dome, supported by an external concrete ring, height 9 m from the ground. The base radius R is equal to 34.55 m, and the dome is 15.7 m deep. The spherical surface has a 46.15 m radius R' (Fig. 1b). The warping of the single layer dome is constituted by timber beams oriented along two orthogonal directions, over a triangulated mesh Fig. 1c and 2a. The first beam order

comprehend 126 principal beams, with a rectangular section 99.2 cm high, while the second order realizes the wind-bracing system. In this case, the rectangular beams are 35 cm height Fig. 1d. The connection are realized by steel plates that encircle a timber cylinder, connected by 60 screwed nails of 6 cm diameter. The connection details are reported in Fig. 2b.

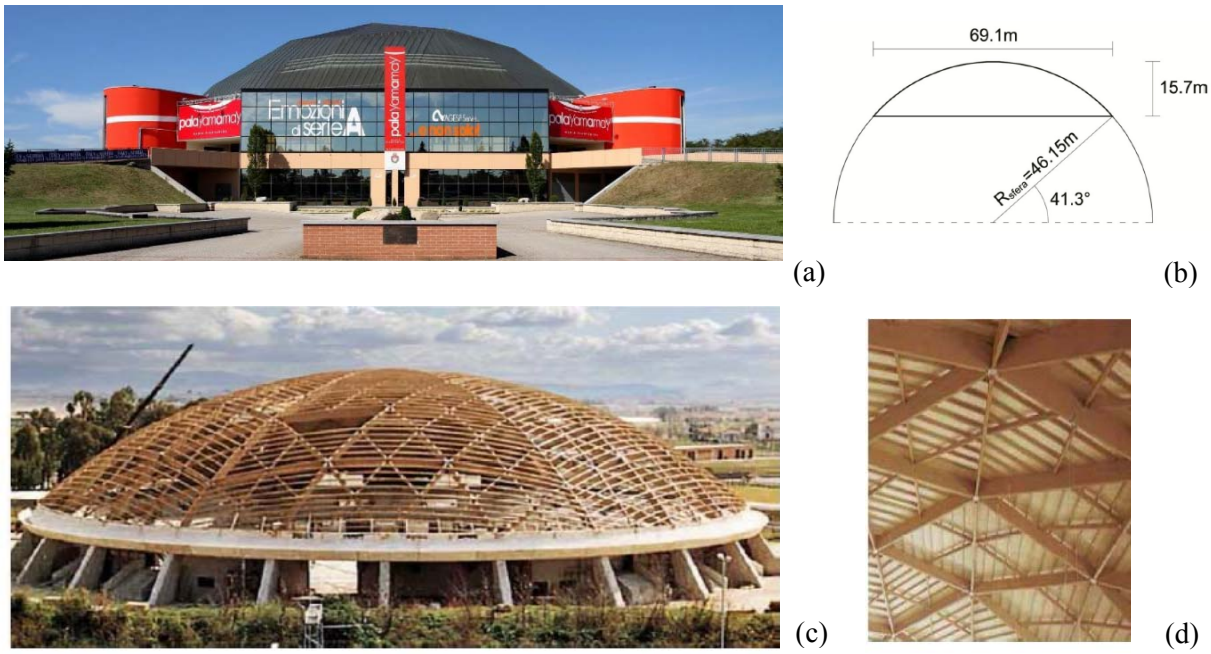

Fig. 1: The Maria Piantanida sport palace, Milan (a); Principal dimensions of the analyzed roof (b); Geometry of the single layer upper view (c); First and second beam order internal view(d).

2. Existent analyses review

The considered dome has been designed following the Italian DIN 1052:85 code, which represents the state of art of timber structures during the building construction. However, the ownership required a further instability assessment of the structure to have a safety check aligned with the new European guidelines (EN14080:2005). A detailed report of these analysis has been reported considering also geometrically non-linear analysis [3]. In this case, an equivalent material properties have been evaluated in order to take into account the degradation of the timber. The principal mechanical characteristics used for this study are reported in Table 1.

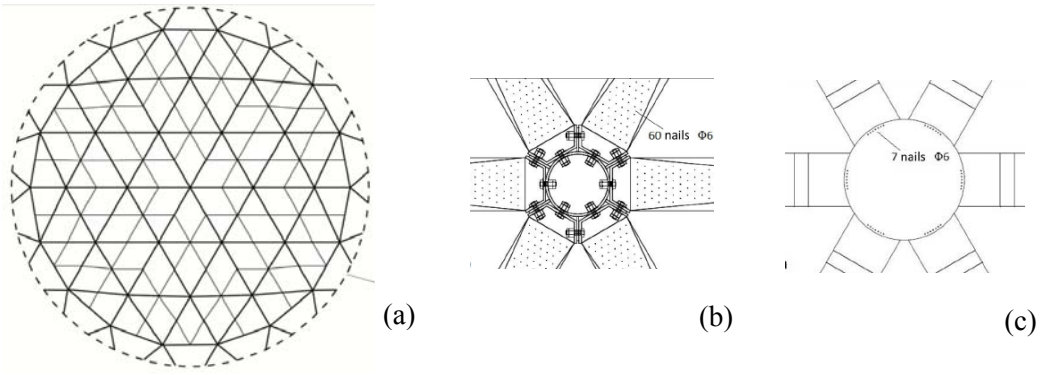

Fig. 2: Warping of the dome grid upper view(a). Bottom view (b) and top view of the connections.

Table 1: Strength and stiffness parameters, EN14080:2005 indications

Mechanical properties	**Characteristic values**	**[MPa]**
Flexure	$f_{m,k}$	24
Parallel tensile stress	$f_{t,0,k}$	14
Orthogonal tensile stress	$f_{t,90,k}$	0.4
Parallel compression	$f_{c,0,k}$	21
Orthogonal compression	$f_{c,90,k}$	2.5
Shear stress	$f_{v,k}$	2.5
Young's modulus, mean value (parallel)	$E_{0,mean}$	11000
Young's modulus (orthogonal)	$E_{0,05}$	7400
Young's modulus (orthogonal)	$E_{90,mean}$	370
Shear modulus	G_{mean}	690

The main instability problem of the structure is represented by the lateral instability of the principal beams. Their substantial difference in base vs. height dimensions evidenced a weakness in sustaining the biaxial flexure induced by the vertical loads. The wind-bracing system should properly contrast this phenomenon, but ad-hoc analyses have not been performed during the design phase. Under the light of these, in the report, cited above [3], the structure has been analyzed considering: (i) the presence or not of the wind-bracing system, (ii) difference in the connection stiffness, (iii) a variable cross-sectional inertia of the bearing elements. In details, Fig. 3 illustrates the load-displacement curves (*F*-*w*), evaluated at the peak node, of the clamped structure in presence of a hinged or clamped wind-bracing system or without any of it. The latter condition shows a consistent reduction of the second limit point coming from a lateral instability of the principal beam skeleton.

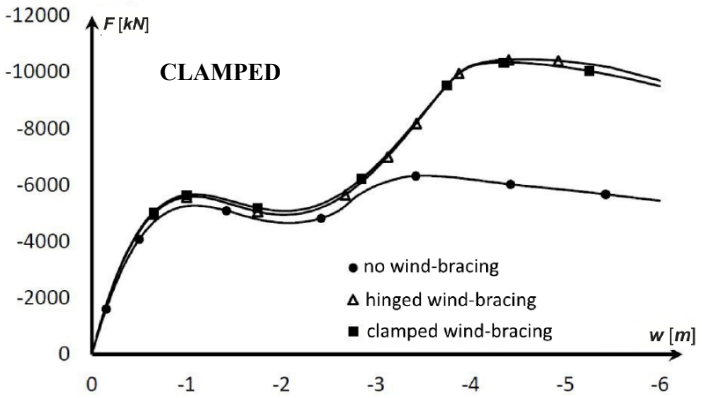

Fig. 3: Load-displacement curves, evaluated at the peak node. The following are case s are considered in comparison: Clamped structure in presence of a hinged or clamped wind-bracing system or without it.

The presence of the wind-bracing system, whatever connected, does not completely exclude the phenomenon, but it happens further along the equilibrium path; this means for a corresponding higher values of load and displacement. It is interesting to note that, if the principal gird is realized with hinged connections, the post-buckling branch has a hardening effect (see Fig. 4). This happens since the lateral instability cannot occur due to the total axial forces regime established in the domes. Under these circumstances, the load displacement curves retraced almost the same equilibrium path. The intermediate connection stiffness were reported in Fig. 5, hence considering each node connected with the same rigidity without any distinction between principal and secondary beam set. In this diagrams, the percentage represents the yieldingness of the connection. Finally, the inertial characteristics influence was studied, in relation to a variable height of the principal beams (Fig. 6a and b).

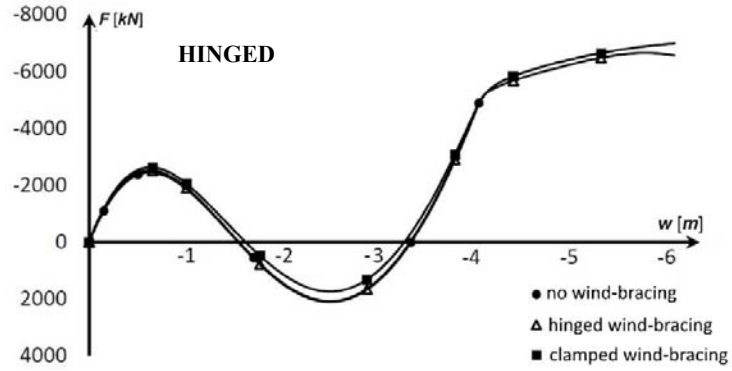

Fig. 4: Equilibrium paths with hinged connections between the principal beams, wind-bracing effect.

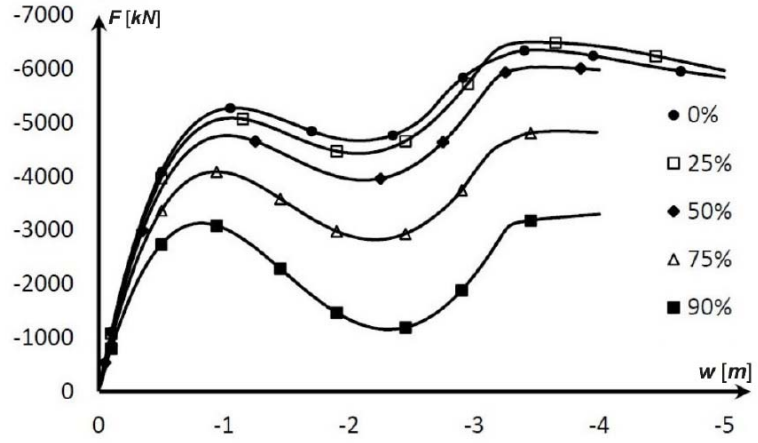

Fig. 5: Equilibrium paths with variable connection stiffness (increasing yieldingness of the connecting nodes).

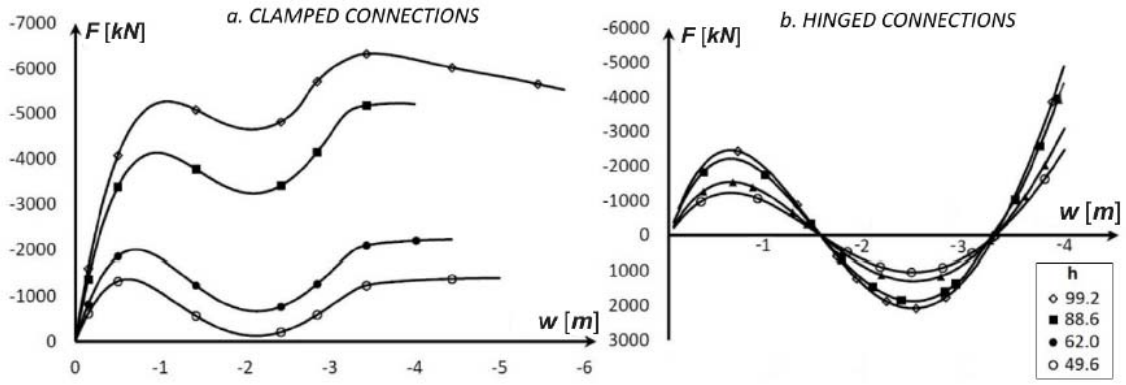

Fig. 6: Equilibrium paths with variable vertical inertia in the case of clamped (a) and hinged (b) connections.

3. Interaction between different instabilities phenomena

Aim of this Section is to extend the investigations about the structural behaviour of the Maria Piantanida sport palace to the instability interaction [1,2,8,9]. Specifically, the imperfection sensitivity was studied through a numerical displacement controlled analysis. By working out these parameters the method adopted evidenced several possible instability interactions. In order to have consistent results with the previous analyses, the same characteristics concerning the material have been adopted (Table 1). It must be underlined that the aim of the analyses reported in this section was to study, as a function of the main parameters, the modalities and the triggers of the interaction effects; moreover, the consequences of these phenomena on the structural behaviour of the structure. The dome is characterized by a shallowness ration, *R/h* equal to 2.22. These parameter will not be varied for all the analyses, while the slenderness effect will be deeply analyzed. Because of the absence of appreciable effects of the bracing system to the snap-through mechanism (the same cannot be said for the buckling modes), the dome was studied considering only the principal beam framework (Fig. 7). In the Figure 7, the beam sections that will be used to for the simulations were reported. Slenderness of the element can be expressed as:

$$\lambda = \sqrt{\frac{AL^2}{I}}$$

where *h* represents the height of the section *L* is the length *A* and *I* represent the area and the moment of inertia. Existing structural properties provided a slenderness value of *41.75*. For the parametric analyses, two other slenderness, equal to *60* and *80*, were considered (Fig. 7b). In Fig. 8 the asymmetric imperfection pattern was reported; deviations were applied along the local vertical axis of the beams.

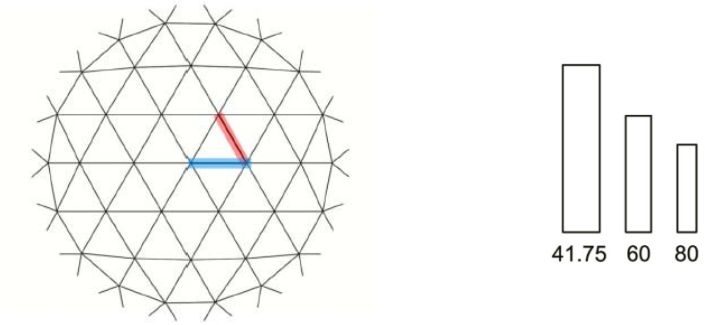

Fig. 7: Principal grid of the dome (a). Shape variation of the adopted sections and the related slenderness λ (b).

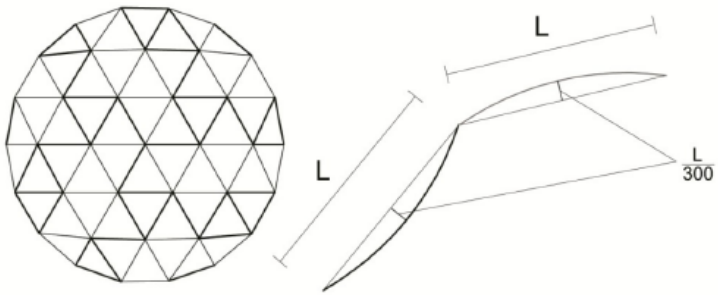

Fig. 8: Asymmetric imperfection pattern, global and local schemes.

Table 2: Slenderness, geometrical characteristics of the considered sections

λ	**b[cm]**	**h[cm]**	**A[cm^2]**	**ΔA[%]**
41.75	22	99.20	2182	-
60	15.31	69.03	1037	51.57
80	11.48	51.77	594	72.77

4. Analysis Results

First analyses regarded the structural and geometrical properties adopted in the building. In Fig. 9a the equilibrium paths, considering hinged connections, were reported as a function of the imperfection existence. It is evident that the interaction problem, as defined in recent studies [1,2,8,9], did not interested the structure (the limit point is essentially coincident). Although, the buckling of the parallel beam induced the not perfect equilibrium path to deviate from the perfect one. A deep investigation evidenced that even this problem did not represent a correct failure of the system: the buckling in the elastic field can be excluded since the meridian beam goes beyond the tensile stress of the element, as reported in Fig. 9c. In spite of this, it is curious how the difference between the perfect and the imperfect systems came only from the buckling of the generic parallel beams (Fig. 9d). As concerning the clamped connections, the equilibrium paths of the dome was reported in Fig. 9b. Because of the almost complete overlapping of the curves, the sole path of the perfect system was traced. Once the first snap-through was over-passed, an unequivocal deviation appeared starting from point ***a***. Extracting the deformed structure at this particular point, it can be observed how this deviation derived from a lateral-flexural instability of the beams. In Table 4, critical load and corresponding reductions were summarized.
In the case of $\lambda = 60$ (increased slenderness) the results are reported in Fig. 10. First of all, as in the previous case the equilibrium paths, considering hinged connections, were reported in the case of presence or absence of imperfections (see Fig. 10a). The increasing of slenderness caused an attenuation of the limit load of the perfect system. Furthermore, an additional reduction came from the rise of an interaction phenomenon which involved the buckling of a meridian beam of the upper dome level. As in the previous case, the second deviation occurred as consequence to the buckling of the upper ring. In order to validate this evidence, the trend of the internal axial forces in the meridian and parallel beam were reported respectively in Fig. 10a and b. In the opposite way respect to the previous case, the material failure involved the parallel beam; this means that for a correct evaluation of the post-peak behaviour, a non-linear analysis of the material is necessary. Differently from what happens to the hinged connections, when the clamps were considered, no interaction phenomena affected the perfect equilibrium path. Also in this case in Table 4, critical load and corresponding reductions were summarized. The last case considered regards a slenderness = 80. the results of an additional increase of the slenderness of the system ($\lambda = 80$) were presented in Fig. 11. In the Fig. 11a the equilibrium paths, considering hinged connections, were reported as a function of the imperfection presence. The increasing of slenderness caused a consistent reduction of the load as a consequence of an interaction phenomenon which involved again the buckling of meridian beams of the upper dome level. For this particular structural arrangement the failure must be solely attributed to instability occurrence. As can be observed in Fig. 11c and d, the critical buckling load substantially reduced the maximum strength of the elements, whatever meridian or beam they were. This particular weakness was immediately identified through this approach, together with a structural comprehension of the mechanical behaviour of each element. Equilibrium paths of the clamped connections domes were reported in Fig. 11b. A small load reduction can be observed in presence of asymmetric imperfections. Although, they cannot be compared to the pinned beams. It is reasonable to think that the slenderness must be further increased to identify significant critical load reductions. In Table 5, the results were summarized accompanied with the corresponding loading reductions.

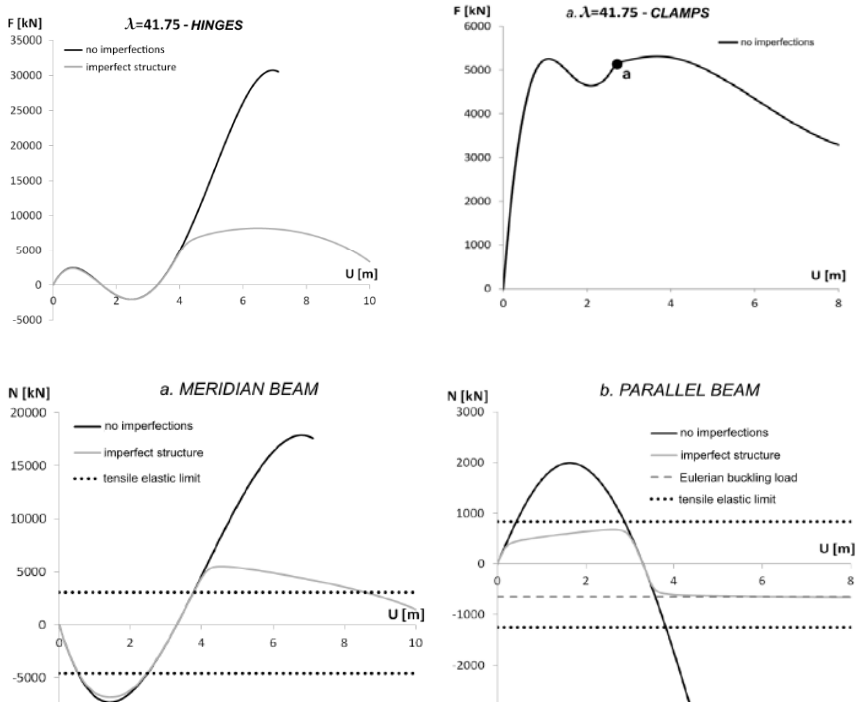

Fig. 9: λ=41.75. Equilibrium paths, hinged connections (a), clamped connections (b). Axial force in the meridian (c) and parallel (d) beams along the considered equilibrium paths.

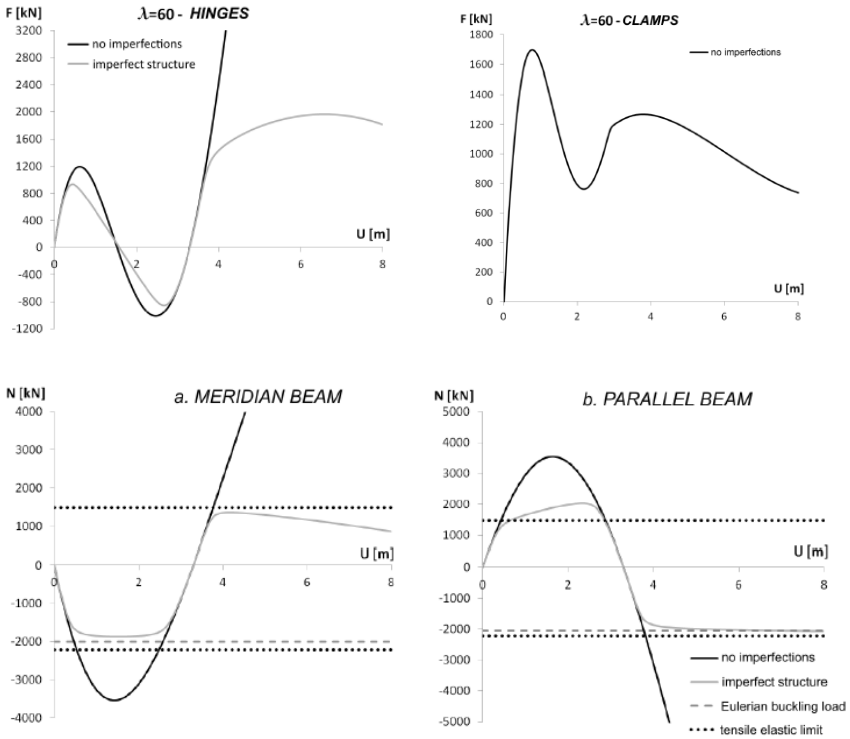

Fig. 10: λ=60. Equilibrium paths, hinged connections (a), clamped connections (b). Axial force in the meridian (c) and parallel (d) beams along the considered equilibrium paths.

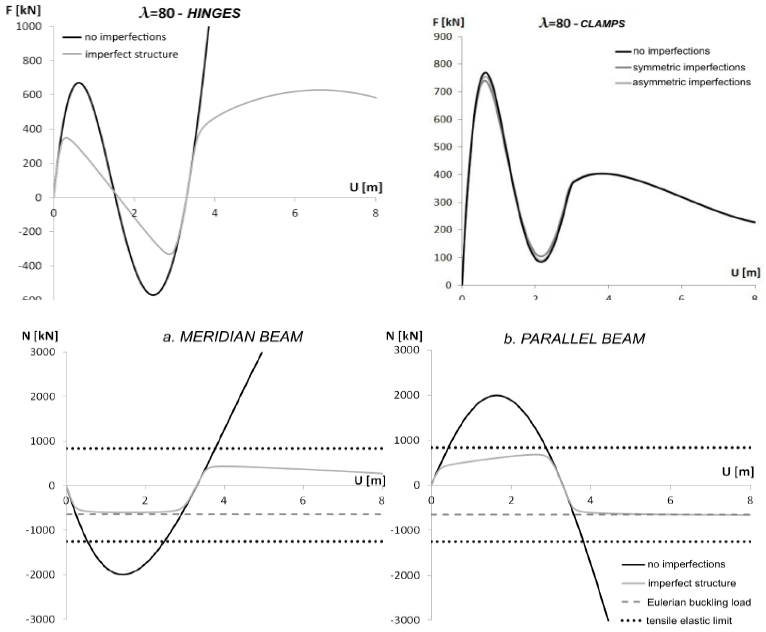

Fig. 11: λ=80. Equilibrium paths, hinged connections (a), clamped connections (b). Axial force in the meridian (c) and parallel (d) beams along the considered equilibrium paths.

Table 4: Load reductions changing the slenderness and the imperfection pattern

λ = 41.75			
		F[kN]	**Load reduction [%]**
hinges	Perfect system	2456.79	–
	Imperfect System	2396.92	–2.44
clamps	Perfect system	5248.46	–
	Symmetric imperfection	5331.35	+1.58
	Asymmetric imperfection	5254.09	+0.11
λ = 60			
		F[kN]	**Load reduction [%]**
hinges	Perfect system	1192.15	–
	Imperfect System	935.92	–21.55
clamps	Perfect system	1696.69	–
	Symmetric imperfection	1670.34	–1.55
	Asymmetric imperfection	1688	+0.47
λ = 80			
		F[kN]	**Load reduction [%]**
hinges	Perfect system	2456.79	–
	Imperfect System	2396.92	–47.94
clamps	Perfect system	5248.46	–
	Symmetric imperfection	5331.35	–3.63
	Asymmetric imperfection	5254.09	–1.73

4. Conclusions

For the clamped structure it is possible to note an evident reduction in the bearing capacity regarding the configuration in which the win bracing is absent. The second peak load observable in the *P-w* path presented a reduction of about 40% respect to the two configurations with hinged or clamped bracing system (Fig. 3). On the other hand no difference can be considered in the case of an hinged grid. As far as the yieldingness increasing of the connections the results have reported in Fig. 5. In this case the interesting consideration is that with a stiffness reduction in the nodes up to the 90% a load bearing capacity depletion of about the 30% in observed. The last, considering an icreasing slendernees of the adopted sections for the principal framework we have a different bahaviour considering the effects of the imperfections. In the case of $\lambda = 41.75$ even if the load reductions appeared to be almost negligible, the structural behaviour variation cannot be neglected. The sharpness of the softening post-buckling branch is a clear evidence of the severity of this collapse. In the case of $\lambda = 60$ the amount of the reduction increased in the case of hinged connections, reaching a load depletion of about 20%. In the last case, for $\lambda = 80$ the load bearing capacity reduction reach a value of about 48%.

Acknowledgements

Dr. Eng. Antonio Comparato is gratefully acknowledged for the analyses performed on the equilibrium paths with variable connection stiffness.

References

[1] Bazzucchi F., Manuello A., Carpinteri A., Interaction between snap-through and Eulerian instability in shallow structures. *Int. J. of Non linear Mechanics*, 2017; **88**; 11 – 20.

[2] Comparato A., Instabilità di una copertura spaziale di grande luce in legno lamellare. Master Thesis, 2014.

[3] Pan D., H., Girhamma U., A., Effect of Ring Beam Stiffness on Behaviour of Reticulated Timber Domes. *Int Journal of Space Structures*, 2005; **20(3)**; 143 – 160.

[4] Sun J., Li H., Nooshin H., Parke G.A.R., Dynamic Stability Behaviour of Lattice Domes with Substructures. *International Journal of Space Structures*, 2014; **29(1)**; 1-7.

[5] Imai K., Miyahara H., Tsujioka S., Shogatsudani K., Furukawa T., Fujimoto M., Fatigue and creep characteristics of wooden space frame joint in *IASS 2016. Spatial Structures in the 21st Century*, Ken'ichi Kawaguchi, Makoto Ohsaki, Toru Takeuchi (ed.), CEDEX Madrid, Spain, 2016.

[6] Nomura K., Nakata K., The structural design of a timber two directional parallel chord truss in *IASS 2016. Spatial Structures in the 21st Century*, Ken'ichi Kawaguchi, Makoto Ohsaki, Toru Takeuchi (ed.), CEDEX Madrid, Spain, 2016.

[7] Furuichi S., Sato J., Design of timber suspension roof pretensioned to reduce deformation under snow load in *IASS 2016. Spatial Structures in the 21st Century*, Ken'ichi Kawaguchi, Makoto Ohsaki, Toru Takeuchi (ed.), CEDEX Madrid, Spain, 2016.

[8] Bazzucchi F., Carpinteri A., Manuello A., Interaction between different instability phenomena in shallow roofing structures affected by geometrical imperfection in *IASS 2016. Spatial Structures in the 21st Century*, Ken'ichi Kawaguchi, Makoto Ohsaki, Toru Takeuchi (ed.), CEDEX Madrid, Spain, 2016.

[9] Manuello A., Bazzucchi F., Carpinteri A., Step-by-step stability analysis of shallow grid shells: Buckling versus snap-through. in *IASS 2016. Spatial Structures in the 21st Century*, Ken'ichi Kawaguchi, Makoto Ohsaki, Toru Takeuchi (ed.), CEDEX Madrid, Spain, 2016.